Arabian Journal of Chemistry (2016) xxx, xxx–xxx

King Saud University

Arabian Journal of Chemistry

www.ksu.edu.sa
www.sciencedirect.com

ORIGINAL ARTICLE

Magnesium incorporated hydroxyapatite nanoparticles: Preparation, characterization, antibacterial and larvicidal activity

Gayathri Udhayakumar [a,*], Muthukumarasamy N. [b], Dhayalan Velauthapillai [c], S.B. Santhosh [d], Vijayshankar asokan [e]

[a] *Department of Chemistry, Coimbatore Institute of Technology, Coimbatore, India*
[b] *Department of Physics, Coimbatore Institute of Technology, Coimbatore, India*
[c] *Faculty of Engineering and Business Administration, Bergen University College, Bergen, Norway*
[d] *Natural drug research laboratory, Department of Biotechnology, School of Bioscience, Periyar University, Salem, India*
[e] *State Key Laboratory of Silicon Materials, School of Material Science and Engineering, Zhejiang University, Hangzhou, China*

Received 21 February 2016; accepted 24 May 2016

KEYWORDS

Microwave irradiation method;
Hydroxyapatite;
Nanoparticles;
Antibacterial activity;
Prokaryotic strains;
Larvicidal activity

Abstract Mosquito-borne diseases cause several deaths every year in tropical and subtropical climate countries. Control of vectors is an alarming problem in today's world due to the resistance matters. In this study magnesium incorporated hydroxyapatite nanoparticles have been synthesized by microwave irradiation method. Magnesium chloride hexahydrate ($MgCl_2{\cdot}6H_2O$) calcium nitrate tetra hydrate ($Ca(NO_3)_2{\cdot}6H_2O$) and disodium hydrogen phosphate (Na_2HPO_4) were used as magnesium, calcium and phosphorous sources to prepare hydroxyapatite nanoparticles. The FT-IR studies show the presence of hydroxyl and phosphate functional groups. The structural properties have been studied using X-ray diffraction (XRD), Field Emission Scanning Electron Microscope (FESEM) and Transmission Electron Microscope (HRTEM). The energy dispersive X-ray analysis (EDAX) revealed the presence of Ca, Mg, P and O in the prepared samples. The antibacterial activity of the as-synthesized nanoparticles was evaluated against two prokaryotic strains, the gram negative bacteria *Escherichia coli* for three different concentrations of as-synthesized nanoparticles and they showed excellent antibacterial activity. The as-synthesized Mg-HAp nanoparticles were tested against fourth instar larvae of *Aedes aegypti*, *Anopheles stephensi*, and *Culex quinquefasciatus* and the nanoparticles exhibited significant mortality against the selected mosquitoes. The observed results suggest that the magnesium incorporated hydroxyapatite nanoparticles have the potential to be used as an effective mosquito larvae control agent against *Ae. aegypti*, *An. stephensi*, and *Cx. quinquefasciatus*. From the detailed literature review it has been observed that no work has been

* Corresponding author.
E-mail address: gayuchem20@gmail.com (G. Udhayakumar).
Peer review under responsibility of King Saud University.

ELSEVIER Production and hosting by Elsevier

http://dx.doi.org/10.1016/j.arabjc.2016.05.010

carried out so far on the larvicidal activity using hydroxyapatite (HAp) nanoparticles and magnesium substituted hydroxyapatite (Mg-HAp) nanoparticles.

1. Introduction

Mosquitoes cause severe disease such as dengue, malaria, chikungunya, filariasis, Japanese encephalitis and leishmaniasis which are endemic in more than 100 countries. Due to mosquito borne disease more than two million people have died throughout the world and 2100 million people are at risk every year (WHO, 2009; Rajakumar and Abdul Rahuman, 2011). *Aedes aegypti* is recognized as a dengue vector and two-fifth of the world population is under risk of dengue (WHO, 2009, 2010). According to the WHO, 2012 survey report 50–100 million people are affected by dengue every year. *Anopheles stephensi* is solely responsible for transmission of malaria which causes morbidity and mortality with nearly three million cases every year (Sharma et al., 2009). Especially, peoples from Middle East and Indian subcontinent were affected by malarial infection severely. *Culex quinquefasciatus* is responsible for lymphatic filariasis commonly known as elephantiasis. In India, more than 553 million people are at risk of infection and are widely distributed in 17 states and 6 union territories (Das et al., 2000). Moreover, 120 million people were affected by lymphatic filariasis (WHO, 2013). Hence Mg-HAp nanoparticles which are less likely to cause ecological damage have been identified as a possible replacement of present insecticides such as permethrin, dieldrin and fenitrothion.

Disease causing microbes of gram negative and gram positive bacteria have become resistant to drug therapy and cause death more than 90 million people every year which is an alarming public health problem nowadays (Stevanovic et al., 2012). Hence there is an urgent need to develop novel bactericides. The antibacterial properties of HAp and Mg-HAp based compounds have been studied (Chung et al., 2006). Since the ion exchanging properties of HAp and Mg-HAp are known to be highly toxic to microbes and exhibit strong biocidal effects, it is currently used to control the bacterial growth and a number of other applications (Ragab et al., 2014). Many researchers have reported the antibacterial activity of HAp and Mg-HAp recently such as Zhao et al., 2016; Jiang et al., 2015; Liu et al., 2012.

Hydroxyapatite (HAp) [$Ca_{10}(PO_4)_6OH_2$] is a material of choice for various biomedical applications such as orthopedic, dentistry, antimicrobial and drug delivery, because of its similarity of composition to mineral phase of the bone, excellent biocompatibility, and ability to promote cellular functions and expression and osteoconductivity. HAp has the ability to integrate in bone structure and support bone in-growth, without breaking down or dissolving (Thamariselvi et al., 2006). Owing to its bioactive property, HAp is widely used in medicine and dentistry as a material for metallic implant coatings, or for bone cavity fillings (Currey, 2001; Thompson et al., 2001). In recent years the application of HAp has extended to various fields due to its excellent properties such as anti-microbial activities (Ragab et al., 2014). However hydroxyapatite does not have good mechanical strength (De With et al., 1981) and has low bioactive property due to its low resorbability (Maria and Daniel, 2005). The HAp lattice can easily accommodate a variety of substituents both cationic and anionic, inducing modifications in the crystallinity, morphology, lattice parameters and stability of the apatite structure. This feature can be used as a powerful tool to prepare materials with specific characteristics mimicking the biological apatites, which are non-stoichiometric and contain structural imperfections and defects as well as foreign ions (Rey, 1998; LeGeros, 1991). Therefore synthetic hydroxyapatite ceramics are doped with small amounts of additives (Mg^{2+}, Zn^{2+}, F^-, Mn^{2+} and CO_3^{2-} ions) in order to improve the mechanical and bioactive property of the implants. The incorporation of magnesium ions into the hydroxyapatite structure leads to significant improvement in the anti-microbial and larvicidal properties of HAp.

There are various methods available to produce nanosize HAp as reported in the literature including sol–gel, hydrothermal, precipitation, spray pyrolysis, solid state reaction method, etc. (Sun et al., 2006; Koumoulidis et al., 2003; Wang et al., 2006; Han et al., 2006; Tas, 2000; Kalita and verma, 2010). In the present study microwave irradiation method has been used to synthesize HAp due to its advantages such as fast reaction rate, simplicity, short reaction time, high reaction selectivity and energy saving. Microwave is an electromagnetic wave of high frequency which consists of alternate magnetic field and electric field. Microwave excitation heats the core and surface of the material homogeneously because microwave energy introduces thermal energy by means of collision between rotating molecules (Siddharthan et al., 2006). Microwave heating has thus been found to be a very convenient thermal source not only in the kitchen but also in a chemical laboratory. Chemists have explored the possibility of the application of a conventional microwave oven to carry out chemical reactions (Rashmi Sanghi, 2000). In the present work, for the first time we have made an attempt to investigate the anti-bacterial and larvicidal activity of microwave synthesized pure HAp and Mg-HAp.

2. Materials and methods

2.1. Chemicals

The chemicals used to synthesize HAp and Mg-HAp are calcium nitrate tetrahydrate ($Ca(NO_3)_2{\cdot}6H_2O$, 98%, Otto), magnesium chloride hexahydrate ($MgCl_2{\cdot}6H_2O$, 97%, Hi-Media), disodium hydrogen phosphate (Na_2HPO_4, 99%, Merck) and ammonium hydroxide (NH_4OH, 25%, Merck). All reagents used were of analytical reagent grade and were used without further purification and deionized water was employed as the solvent throughout the experiments.

2.2. Synthesis

Pure HAp and Mg-HAp were synthesized by microwave irradiation method. In a typical procedure for the synthesis of pure HAp, 10 mL of 0.15 M sodium dihydrogen phosphate was added to 10 mL of 0.25 M calcium nitrate tetrahydrate drop by drop to produce a colloidal solution while Ca/P ratio was maintained at 1.67. The molar ratios of the chemical elements of reactants used in the preparation of the powders are reported in Table 1.

Table 1 Molar ratios of the reactants used in the preparation.

Sample name	Ca	P	Mg/Ca	(Ca + Mg)/P
HAp	1.09	0.53	0	1.62
Mg-HAp	0.37	0.38	0.56	1.31

Please cite this article in press as: Udhayakumar, G. et al., Magnesium incorporated hydroxyapatite nanoparticles: Preparation, characterization, antibacterial and larvicidal activity. Arabian Journal of Chemistry (2016), http://dx.doi.org/10.1016/j.arabjc.2016.05.010

The reaction for the formation of pure HAp is

$$10\,Ca(NO_3)_2\cdot 4H_20 + 6Na_2HPO_4 + 8NH_4OH \rightarrow Ca_{10}(PO_4)_6(OH)_2 + 8NH_4NO_3 + 12NaNO_3 + 10H_2O$$

The pH of the final solution was adjusted to lie in the range of 9–11 by adding ammonium hydroxide solution. After stirring for 4 h the reaction solution was kept in a microwave oven (2.45 GHz, ONIDA, INDIA) at 720 W power. The obtained white precipitate was washed using deionized water to remine NH_4^+, Na^{2+} and NO_3^- ions were removed by washing the precipitate. The obtained white precipitate was dried in a muffle furnace at 600 °C for 3 h.

For the synthesis of Mg-HAp, (0.25 –A) M Ca $(NO_3)_2{\cdot}6H_2O$, 0.125 M $MgCl_2{\cdot}6H_2O$ and 0.15 M Na_2HPO_4 were used. The reaction for the formation of Mg-HAp is

$$10-A\,Ca(NO_3)_2\cdot 4H_20 + AMgCl_2\cdot 6H_2O + 6Na_2HPO_4 + 8NH_4OH \rightarrow Ca_{10-A}(PO_4)_6(OH)_2 + 8NH_4NO_3 + 12NaNO_3 + [6+4(10-A+6A)]H_2O$$

2.3. Characterization techniques

The final product was crushed into fine powder using a mortar and pestle. The resultant powder was then studied using various techniques. The FTIR spectral characterization was performed for functional group analysis of the as-synthesized HAp and Mg-HAp samples by using Nicolet 380 FTIR spectrophotometer over the range from 4000 to 400 cm^{-1} at 4 cm^{-1} resolutions and 32 scans. For this, a small amount of above samples was blended with KBr and then pressed into disks for the analysis.

The phase composition, purity, crystallinity size and lattice parameter of the as synthesized HAp and Mg-HAp nanoparticles were studied using XRD (Philips X'pert diffractometer – PANalytical Inc., USA) equipped with X' cellarator using Cu Kα radiation generated at 35 kV and 25 mA. The crystallite size of the samples was calculated from the XRD pattern with standard data compiled by the International Center for Diffraction Data (ICDD) using the Debye–Scherrer's approximation (Pang and Bao, 2003).

$$D = \frac{K\lambda}{\beta\cos\theta} \quad (1)$$

where D is the crystallite size (in nm), λ is the wavelength of Cu Kα radiation (λ = 1.5418 A), β is the full width at half maximum (FWHM) for the diffraction peak under consideration (in radian), θ is the diffraction angle (°) and K is the broadening constant.

Lattice parameters a and c were calculated from peaks using the standard hexagonal unit cell plane spacing relationship by using following equation (Mansur et al., 2012):

$$\frac{1}{d^2} = \frac{4}{3}\frac{(h^2+hk+k^2)}{a^2} + \frac{l^2}{c^2} \quad (2)$$

where d is the distance between adjacent planes in the set of Miller indices ($h\,k\,l$).

The morphology and elemental composition of the as-synthesized samples of HAp and Mg-HAp were studied using FESEM (Curl J diss Supra 40-2007, Germany) operated at an accelerating voltage of 15 kV equipped with EDAX. The samples for FESEM examination were prepared by placing the powders on the conductive carbon tape and they were further sputter coated with gold. High resolution transmission electron microscopy (HRTEM – FEI Tecnai G2 F20) at an operating voltage of 200 kV was employed to obtain the structural information.

3. Antibacterial assay

3.1. Bacterial strains

Cultures of *Escherichia coli* and *Staphylococcus aureus* were obtained from the School of Biosciences, Department of Biotechnology, Periyar University, Tamil Nadu, India. Strains were maintained on nutrient agar for further study.

3.2. Agar well diffusion assay

The antibacterial activity of as synthesized samples was tested by the standard agar well diffusion method. Wells were made using a sterile cork borer (6 mm). Bacterial suspensions were prepared by growing a single colony overnight in Luria–Bertani broth with a turbidity of 0.5 McFarland standards and were swabbed onto the plate which were previously seeded by one of the tested pathogenic bacteria. Positive and negative controls as well as the different concentrations of the synthesized samples (50, 75 & 100 µl) were loaded on marked wells with the help of micropipette and plates were incubated at 37 °C for 24 h. The zone of growth inhibition was measured using a ruler and expressed in mm. All the experiments were performed in triplicate under aseptic condition (Abdel Raouf et al., 2013; Velmurugan et al., 2014).

3.3. Larvicidal activity

Larvicidal bioassay was carried out according to WHO (1996) protocols with some modifications. Twenty-five numbers of fourth instar larvae were introduced into a 500 mL glass beaker containing 249 mL of dechlorinated water and the desired concentrations of Mg HAp and HAp. The number of dead larvae was counted after 24 h of exposure. The percentage mortality and LC_{50}, LC_{90} values were calculated from the average of three replicates. As synthesized Mg HAp toxicity tests were conducted using a multi concentrations test, consisting of a control, different concentrations of Mg HAp. Each test was performed by placing 25 mosquito larvae into 250 mL of sterilized double distilled water with Mg HAp into a glass beaker. Nanoparticle solution was diluted using double distilled water as a solvent according to the desired concentrations (30, 60, 90, 120 and 150 µg/ml). The control was set up using dechlorinated water. Each test was performed three times for accurate results. Mortality was assessed after 24 h to determine the acute toxicities on fourth instar larvae of mosquitoes.

3.4. Dose–response bioassay

Based on the preliminary screening results, Mg HAp and HAp were subjected to dose–response bio assay for larvicidal activity against the fourth instar larvae of three mosquitoes.

Please cite this article in press as: Udhayakumar, G. et al., Magnesium incorporated hydroxyapatite nanoparticles: Preparation, characterization, antibacterial and larvicidal activity. Arabian Journal of Chemistry (2016), http://dx.doi.org/10.1016/j.arabjc.2016.05.010

Different concentrations of Mg HAp and HAp (30, 60, 90, 120 and 150 μg/mL) were prepared. The numbers of dead larvae were counted after 24 h of exposure. The LC_{50} and LC_{90} values were calculated from the average of three replicates.

3.5. Statistical analysis

The average larval mortality data were subjected to probit analysis for calculating LC_{50} and LC_{90} (lethal concentration) values and their statistics at 95% confidence limits of upper confidence limit (UCL) and lower confidence limit (LCL) values were estimated by fitting a probit regression model. All the analyses were calculated using the SPSS (Statistical Package of Social Sciences) software package 16.0 version. Results with $p < 0.05$ were considered to be statistically significant.

4. Result and Discussion

4.1. FT-IR Analysis

FT-IR spectra of the as-synthesized HAp and Mg-HAp nanoparticles are shown in Fig. 1. The characteristic sharp bands are present at 1026 cm^{-1}, 1032 cm^{-1}, for HAp and Mg-HAp and they correspond to the stretching mode of phosphate groups (Sargin et al., 1997; Ramanan and Ramannan, 2004). The bands present at 607 cm^{-1}, 563 cm^{-1} & 609 cm^{-1}, 563 cm^{-1} are due to bending mode of P–O bonds in phosphate group (Russell et al., 1996). As well as the small peak located at 969 cm^{-1} indicates symmetric stretching vibrations normally associated with a P–O mode (Gérrard et al., 2016). Thus the presence of PO_4^{3-} group in HAp is almost confirmed from FT-IR studies. The peaks around 1749 cm^{-1} and 1736 cm^{-1} for Hap and Mg-Hap were attributed to the absorbed water molecule (JunfengJia et al., 2010). Moreover the weak peaks observed around 3571 cm^{-1} and 3554 cm^{-1} for HAp and Mg-HAp are due to the presence of O–H bond. This peak is mainly due to O–H stretching vibration in HAp. Furthermore, the broad stretching band present at 1367 cm^{-1} for HAp and Mg-HAp is attributed to the carbonate group (Iafisco et al., 2010). As well as the weaker peak located at 832 cm^{-1} is associated with a carbonate group and clearly indicates the presence of carbonates in the sample. The presence of carbonate ions in the sample is a consequence of atmospheric carbon dioxide interacting with HAp precursors in the synthesis solution (Panda et al., 2003; Wang et al., 2006). The FTIR spectrum of Mg-HAp nanoparticles (Fig. 1(b)) shows a similar structure as that of pure HAp (Zhang et al., 2011; Bigi et al., 2007), but with a change in the IR wave numbers of bands. Moreover Mg-HAp powder exhibits broader bands when compared to pure HAp (Landi et al., 2008). Thus the obtained FT-IR spectra confirmed the formation of Mg-HAp nanoparticles and no other impurities were identified.

4.2. Morphological and structural analysis

The XRD pattern of the as-synthesized HAp and Mg-HAp nanoparticles is shown in Fig. 2. The diffraction peaks correspond to HAp and are in good agreement with the standard data for HAp (JCPDS ICDD card No. 09-0432). The diffraction peaks are sharp and narrow implying that synthesized HAp exhibits good crystallinity. The X-ray diffraction peaks of Mg-HAp are slightly shifted when compared to that of HAp and this shift is due to the incorporation of Mg in HAp matrix. The 2Θ values for the HAp peaks were found to be 29.13, 32.17, 34.37, 39.59, 46.71, 48.17, 49.69, 53.51 and 64.51 respectively and the planes corresponding to the 2Θ values were (210), (112), (202), (310), (222), (312), (213), (402), (004) and (323). The observed peaks were comparable to the early report of Baikie et al. (2009) and Kazin et al. (2007). These peaks experienced a shift toward the lower diffraction angle which may be occurred due to the influence of the magnesium ions substitution that leads to the distortion in the HAp lattice. (Gopi et al., 2014). The lattice parameter for both HAp and Mg-HAp is shown in Table 2. It is noticed that substitution of Mg resulted in small change in apatite structure, with its smaller ionic radius (0.65 Å), and Mg substitution for Ca causes a reduction in the lattice parameters of stoichiometric hydroxyapatite (Iafisco et al., 2014). The degree

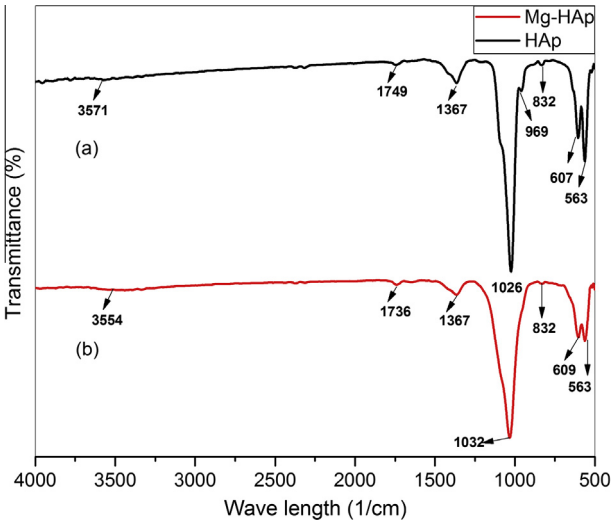

Figure 1 FT-IR spectra of (a) HAp and (b) Mg-HAp nanoparticles.

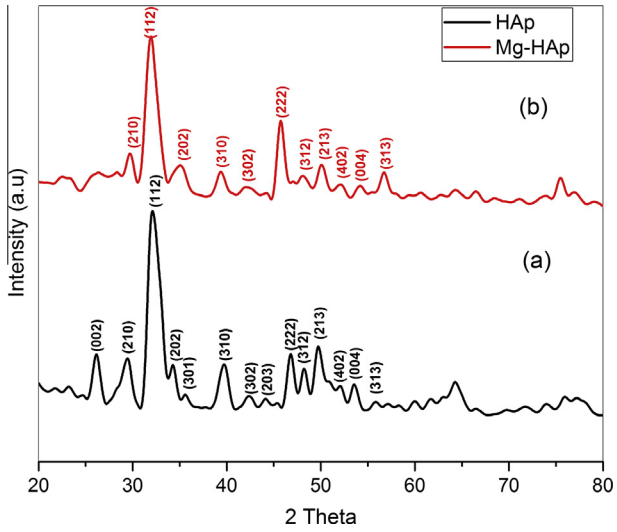

Figure 2 Powder XRD pattern of (a) HAp and (b) Mg-HAp nanopoarticles

Table 2 Lattice parameter of HAp and Mg-HAp.

Sample name	2θ	d spacing	h	k	l	$a = b$ (Å)	c (Å)
HAp	32.17	2.7802	1	1	2	9.5346	6.8438
	46.71	1.9431	2	2	2	9.4436	6.8444
	48.17	1.8876	3	1	2	9.4254	6.8445
	49.69	1.8333	3	2	1	9.5779	6.8445
Average						9.4953	6.8443
Mg-HAp	31.97	2.7972	1	1	2	9.0241	7.1296
	45.65	1.9857	2	2	2	9.5643	7.1296
	48.15	1.8883	3	1	2	9.2699	6.8466
	50.11	1.8189	3	2	1	9.4956	6.8619
Average						9.3385	6.9919

of crystallinity of HAp and Mg-HAp is shown in Table 3. The substitution of Mg in HAp lattice reduced the degree of crystallinity of HAp and it is evident that incorporation of Mg into HAp structure does not encourage the crystallization of hydroxyapatite (HAp – 9.04 nm & Mg-HAp – 6.59 nm) (Landi et al., 2000). Moreover the results clearly showed that the average crystallite size of HAp decreased because of Mg substitution. Mg incorporated into the HAp structure made the grain irregular and the remaining Mg was adsorbed on the surface of HAp which inhibits the grain growth (Geng et al., 2015).

The surface morphology of the HAp and Mg-HAp nanoparticles has been investigated using FESEM and the images are shown in Fig. 3. FESEM images give the direct information about the shape and size of the crystallinity in the as-synthesized samples. The scanning electron microscope image of HAp shows the presence of nanorods. The nanorods have not grown vertically, and it has grown in such a way covering the entire volume and has made the sample to exhibit a smooth surface morphology. The scanning electron microscope image of Mg-HAp shows that length of the nanorods has got reduced due to the incorporation of Mg. This reduction of length of Mg-HAp nanorods is due to the fact that Mg inhibits HAp crystallization in solution (Bertoni et al., 1998). Energy dispersive X-ray analysis was carried out to identify the elemental composition of the HAp and Mg-HAp nanoparticles. Fig. 4 shows EDAX spectra of the as-synthesized samples. EDAX pattern indicates the presence of Ca, Mg, P, O, C and Cl in the as-synthesized nanoparticles. Chlorine could be a possible remnant of the reaction, not completely removed through washing. The presence of carbon is mainly due to the carbon tape used to mount the samples.

HRTEM images for HAp and Mg-HAp nanostructures are displayed in Fig. 5(a, b) and (c, d), respectively. On the first observation, HAp contains uniformly shaped nanorods while Mg-HAp contains nanorods of varying shapes and nanoparticles distributed throughout the samples, which is also evident from FESEM images shown in Fig. 3a and b. Typical HRTEM

Table 3 Crystallite size of synthesized powders.

Sample	Crystallite size (nm)			
	112	312	310	Average
HAp	5.5045	14.510	7.1306	9.0484
Mg-HAp	5.0250	8.2886	6.4706	6.5947

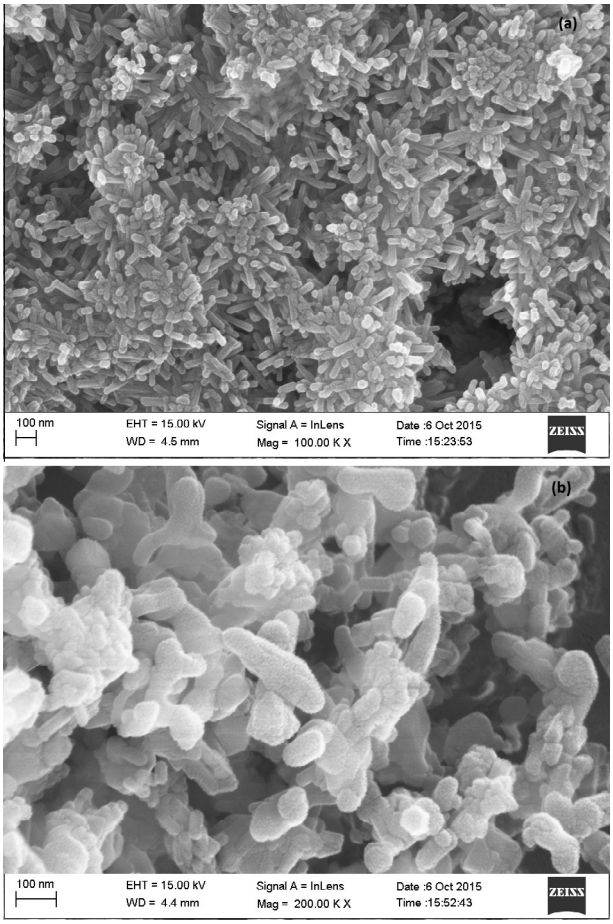

Figure 3 FESEM images of (a) pure HAp and (b) Mg substituted HAp nanoparticles.

image of HAp in Fig. 5a shows that it contains nanorods, most of which are around 175–200 nm length and 20–30 nm dia (shown by arrow 1). In addition, it also contains nanorods around 50 nm length and 20–30 nm dia (shown by arrow 2). HRTEM image in Fig. 5b shows that the nanorods are crystalline in nature and the calculated lattice spacing is around 0.80 nm. Typical TEM image of Mg-HAp in Fig. 5c shows that it contains nanorods, most of which are around 50–150 nm length and 20–30 nm dia and the calculated lattice spacing of the nanorods is around 0.70 nm. The decrease in the lattice spacing of Mg-HAp compared to HAp is possibly due to the incorporation of Mg ion, which also matches with arguments explained with XRD peaks above. In addition, Mg-HAp also contains nanoparticles of near spherical nature, which is also evident from FESEM image Fig. 3b.

4.3. Antibacterial activity

The antibacterial activity of as-synthesized samples with three different concentrations (75, 50 and 100 µl) from prepared sample was tested against two bacterial strains by agar well diffusion method. Based on the data obtained from this study, no zone of inhibition was observed against *staphylococcus aureus* for all the concentrations. However, the positive control ciprofloxacin was effective against *S. aureus* at the concentration of

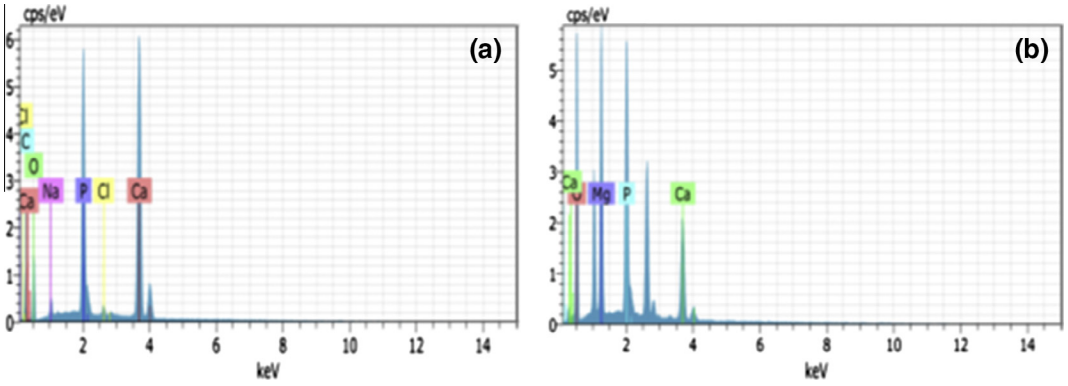

Figure 4 EDAX spectra of (a) HAp and (b) Mg-substituted HAp nanoparticles.

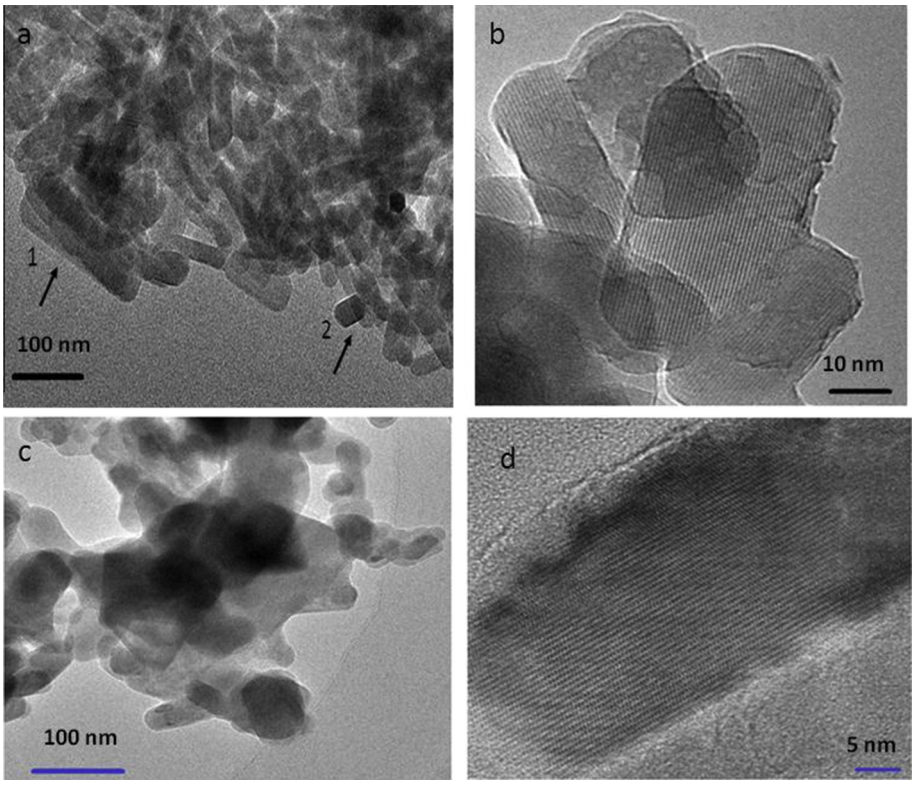

Figure 5 HRTEM images of (a and b) pure HAp and (c and d) Mg substituted HAp nanoparticles.

1 mg/mL and the negative control DMSO does not have any activity against both gram-positive and negative-bacteria. The gram negative bacteria *E. coli* for three different concentrations of synthesized nanoparticles and ciprofloxacin showed excellent antibacterial activity (Fig. 5). The highest zone of inhibition was observed in gram-negative bacteria. There are numerous reasons to explain the present results of antibacterial tests. Most importantly the cell wall of gram negative bacteria is made up of the thin peptidoglycan and lipopolysaccharide layer which influences the permeability of molecules present in the synthetic chemicals that cause respiratory functions culminating in cell death. Previous studies reported that the ions present in the nanoparticles react with SH groups of proteins and play a vital role in inactivation of bacteria (Guzman et al., 2012). Also some studies reported to uncouple respiratory electron transport from oxidative phosphorylation which inhibits respiratory chain enzymes and interferes with membrane permeability to phosphate and protons (Feng et al., 2000). The mechanisms behind the antibacterial activity of nanoparticles were not yet completely elucidated. Up to now few common mechanisms were suggested for antibacterial activity of silver nano particles, and there are uptake of free silver ions which disrupt the DNA replication and ATP production, Reactive Oxygen species (ROS) formation, and damage to cell membranes directly (Sahayaraj and Rajesh, 2011). It may assume to be the same action by HAp and Mg-HAp nanoparticles. The possible reason for the lack of zone of inhibition in gram positive bacteria might be due to the thick cell wall, consisting of murein, lipoteichoic acids and mucopeptides and another possible reason for lack of

Please cite this article in press as: Udhayakumar, G. et al., Magnesium incorporated hydroxyapatite nanoparticles: Preparation, characterization, antibacterial and larvicidal activity. Arabian Journal of Chemistry (2016), http://dx.doi.org/10.1016/j.arabjc.2016.05.010

activity is might be that the molecules present in the synthetic chemicals may not be active against all the bacteria. Ragab et al. (2014) have reported that the anti-microbial activity of HAp nanoparticles has the potential to control microbes and they observed 14.9 + 0.97 mm zone of inhibition against gram negative bacteria and 9.0 + 2.56 mm zone of inhibition against gram positive bacteria. We observed 16.38 ± 1.22 mm zone of inhibition against gram negative bacteria and 3.91 ± 0.07 mm zone of inhibition against gram positive bacteria. This previous study strongly supports our present findings.

4.4. Larvicidal activity

The present study shows that the synthesized Mg-HAp has a highest mortality in all the three species when compared to the HAp with lowest LC_{50} and LC_{90} values. The results of larvicidal activity of Mg-HAp were tested against fourth instar larvae of *Ae. aegypti*, *An. stephensi*, and *Cx. quinquefasciatus*. The larvicidal study showed the following LC_{50} and LC_{90} values: *Ae. aegypti* (LC_{50} 10.09 μg/mL; LC_{90} 21.75 μg/mL), *An. stephensi* (LC_{50} 13.99 μg/mL; LC_{90} 26.21 μg/mL) and *Cx. quinquefasciatus* (LC_{50} 16.21 μg/mL; LC_{90} 33.43 μg/mL) respectively (Table 4). Percentage of mortality was calculated (Fig. 6). This result is comparable to earlier reports of Santhoshkumar et al. (2011) who observed that the highest mortality was found in methanol, aqueous, and synthesized AgNPs, which used *N. nucifera* plant extract against the larvae of *An. subpictus* (LC_{50} = 8.89, 11.82, and 0.69 ppm; LC_{90} = 28.65, 36.06, and 2.15 ppm) and against the larvae of *Cx. quinquefasciatus* (LC_{50} = 9.51, 13.65, and 1.10 ppm; LC_{90} = 28.13, 35.83, and 3.59 ppm), respectively. Recently, many researchers have started to analyze the larvicidal activity of different synthetic and plant mediated nanoparticles. For example, the highest larval mortality was found in the

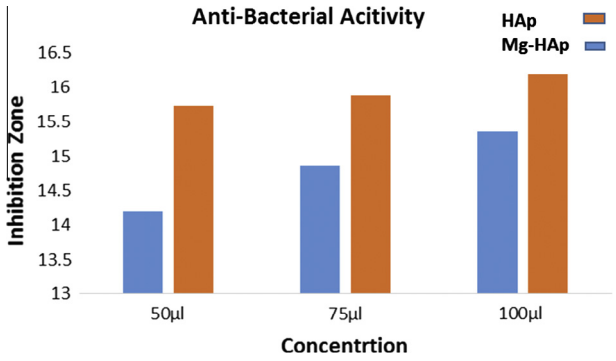

Figure 6 Antibacterial activity of HAp and Mg-HAp nanoparticles.

synthesized AgNPs against the first to fourth instar larvae with LC_{50} values of 10.14, 16.82, 21.51, and 27.89 ppm, respectively; LC_{90} values of 31.98, 50.38, 60.09, and 69.94 ppm, respectively (Priyadarshini et al., 2012). Larvicidal activity of synthesized AgNPs utilizing an aqueous extract from *Eclipta prostrata* was observed in crude aqueous and synthesized AgNPs against *Cx. quinquefasciatus* (LC_{50} = 27.49 and 4.56 mg/L; LC_{90} = 70.38 and 13.14 mg/L) and against *An. subpictus* (LC_{50} = 27.85 and 5.14 mg/L; LC_{90} = 71.45 and 25.68 mg/L), respectively (Rajakumar and Abdul Rahuman, 2011). The obtained highest larvicidal activity in the present study is due to the incorporation of magnesium ions into the hydroxyapatite which makes the nanoparticle structure more compatible which can easily penetrate into the cuticle layer of the mosquitos and rupture the cell. Our findings long-established the mechanisms of larvicidal activity. According to Sap-Iam et al., (2010) the nanoparticles may penetrate through the larval membrane which causes the death of larva. As well as Sondi and Salopek, 2004; Choi et al., 2008; Rai

Table 4 Larvicidal activity of HAp against fourth instar mosquito larvae of *Ae. aegypti*, *An. stephensi*, and *Cx. quinquefasciatus* of 24 h observation.

Mosquitoes	Concentration of Mg HAp	24-h Mortality (%) ± SD	LC_{50} μg/mL (LCL-UCL)	LC_{90} μg/mL (LCL-UCL)	X^2
Aedes aegypti	Control	0.0 ± 0.0			
	30	52.0 ± 0.0			
	60	61.3 ± 2.3	50.24	106.42	
	90	77.3 ± 2.3	(39.81–59.58)	(93.95–124.54)	29.11*
	120	90.6 ± 2.3			
	150	100 ± 0.0			
Anopheles stephensi	Control	0.0 ± 0.0			
	30	45.3 ± 2.3			
	60	61.3 ± 2.3	58.79	133.60	
	90	72.0 ± 4.0	(46.24–69.95)	(117.33–158.20)	28.29*
	120	81.3 ± 2.3			
	150	90.6 ± 2.3			
Culex quinquefasciatus	Control	0.0 ± 0.0			
	30	34.6 ± 2.3			
	60	46.6 ± 2.3	79.30	171.16	
	90	57.3 ± 2.3	(70.11–88.59)	(153.93–195.59)	22.97*
	120	70.6 ± 2.3			
	150	78.6 ± 2.3			

UCL: upper confidence limit, LCL: lower confidence limit, χ^2: Chi-square test, significant at $p < 0.05$ level.
* The average value of triplicate.

Table 5 Larvicidal activity of Mg-HAp against fourth instar mosquito larvae of *Ae. aegypti, An. stephensi* and *Cx. quinquefasciatus* of 24 h observation.

Mosquitoes	Concentration of HAt	24-h Mortality (%) ± SD	LC_{50} µg/mL (LCL-UCL)	LC_{90} µg/mL (LCL-UCL)	X^2
Aedes aegypti	Control	0.0 ± 0.0			
	30	49.3 ± 6.1	10.09	21.75	31.97*
	60	64.0 ± 4.0	(7.87–12.10)	(19.08–25.72)	
	90	74.6 ± 2.3			
	120	89.3 ± 2.3			
	150	100 ± 0.0			
Anopheles stephensi	Control	0.0 ± 0.0			
	30	33.3 ± 2.3	13.99	26.21	23.52*
	60	45.3 ± 4.6	(12.64–15.33)	(24.17–28.87)	
	90	58.6 ± 2.3			
	120	78.6 ± 2.3			
	150	100 ± 0.0			
Culex quinquefasciatus	Control	0.0 ± 0.0			
	30	36.0 ± 4.0	16.21	33.43	19.57*
	60	44.0 ± 4.0	(14.47–17.98)	(30.24–37.86)	
	90	56.0 ± 4.0			
	120	72.0 ± 4.0			
	150	80.0 ± 0.0			

UCL: upper confidence limit, LCL: lower confidence limit, χ^2: Chi-square test, significant at $p < 0.05$ level.
* The average value of triplicate.

et al., (2009) reported that the nanoparticles in the intracellular space can bind to proteins which contain sulfur or phosphorus containing compound like DNA which leads to the denaturation of some enzymes and some organelles. Subsequently, the dropping of membrane permeability and disturbance in proton motive force required for ATP construction are induced which affects the cellular function and finally leads to cell death (Lok et al., 2006).

Similarly the results of larvicidal activity of HAp were tested against fourth instar larvae of *Ae. aegypti*, *An. stephensi*, and *Cx. quinquefasciatus* are presented in (Table 5). The LC_{50} and LC_{90} values of HAp against fourth instar larvae of *Ae. aegypti* showed lowest LC_{50} and LC_{90} values (LC_{50} 50.24 µg/mL; LC_{90} 106.42 µg/mL) followed by *An. stephensi* (LC_{50} 58.79 µg/mL; LC_{90} 133.60 µg/mL) and *Cx. quinquefasciatus* (LC_{50} 79.30 µg/mL; LC_{90} 171.16 µg/mL) respectively (Fig. 7). Govindarajan (2010) has reported that the study of crude extract of *Sida acuta* against the three important mosquitoes yields LC_{50} values which lie in the range between 38 and 48 mg/L. This result is comparable to our findings. The leaf petroleum ether, flower methanol extracts of *Cryptocoryne auriculata*, flower methanol extracts of *Leucas aspera* and *Rhinacanthus nasutus*, leaf and seed methanol extracts of *Solanum torvum*, and leaf hexane extract of *Vitex negundo* were evaluated for larvicidal activity by Kamaraj et al. (2009) and they have reported LC_{50} values of 44.21, 44.69, 53.16, 41.07, 35.32, 28.90, and 44.40 ppm, respectively. The possible reason for the significant larvicidal activity of HAp might be the ion exchange properties of HAp which strongly supports to disturb the regular mechanism of cell. From the present observations both HAp and Mg-HAp

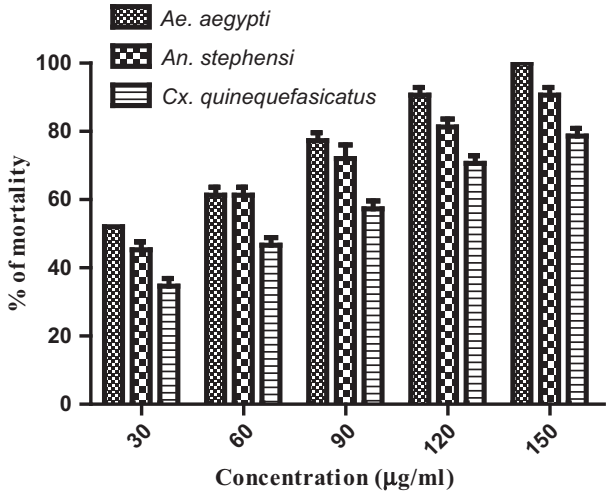

Figure 7 The percentage mortality of HAp against *Ae. aegypti*, *An. stephensi* and *Cx. quinquefasciatus*.

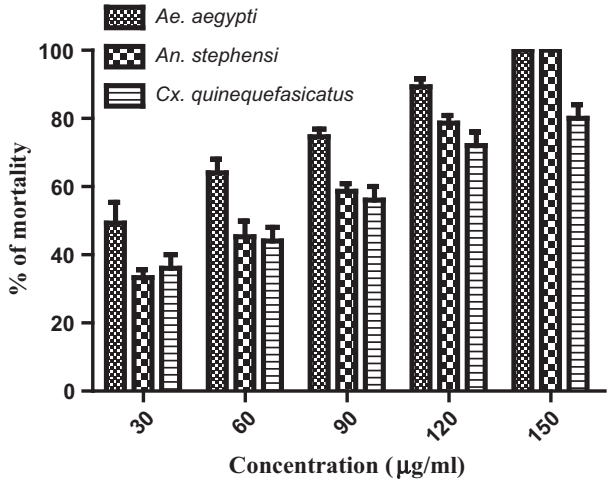

Figure 8 The percentage mortality of Mg-HAp against *Ae. aegypti*, *An. stephensi* and *Cx. quinquefasciatus*.

showed significant larvicidal activity. When compared with HAp, Mg-HAp showed excellent larvicidal activity in all the three species. This effective larvicidal activity might be due to the O–H bond, phosphate group presence in the HAp and Mg-HAp (see Fig. 8).

5. Conclusion

In summary, pure and Mg substituted hydroxyapatite was successfully prepared by microwave irradiation method. Magnesium incorporation affects the crystallinity and morphology of pure HAp nanoparticle and is evident from XRD and FESEM. FESEM and HRTEM images shows pure HAp that is well crystallized and regular shape of nanorods. Due to the incorporation of Mg, the crystallinity becomes smaller, irregular and more agglomerates. Moreover FTIR analysis of the Mg-HAp nanoparticles gives broader spectra compared to pure HAp. Further, we demonstrated the possible application of HAp and Mg-HAp in the medical field as it shows significant antibacterial activity against human pathogenic bacteria as well as excellent larvicidal activity against selected mosquitoes. We strongly conclude that the as synthesized Mg-HAp can be used as a better larvicidal agent.

References

Abdel Raouf, N., Al-Enazi, N.M., Ibraheem, I.B.M., 2013. Green biosynthesis of gold nanoparticles using *Galaxaura elongata* and characterization of their antibacterial activity. Arabian J. Chem. http://dx.doi.org/10.1016/j.arabjc.2013.11.044.

Baikie, T., Ng, G.M., Madhavi, H., Pramana, S., Blake, S.S., Elcombe, K.M., White, T.J., 2009. The crystal chemistry of the alkaline earth apatites $A_{10}(PO_4)_6Cu_xO_y(H)_z$ (A = Ca, Sr and Ba. RSC Dalton Trans. 34, 6722–6726.

Bertoni, E., Bigi, A., Cojazzi, G., Gandolfi, M., Panzavolta, S., Roveri, N., 1998. Nanocrystals of magnesium and fluoride substituted hydroxyapatite. J. Inorg. Biochem. 72, 29–35.

Bigi, A., Boanini, E., Capuccini, C., Gazzano, M., 2007. Strontium-substituted hydroxy-apatite nanocrystals. Inorg. Chim. Acta 360, 1009.

Chung, R., Hsieh, M., Huang, C., Perng, L., Wen, H., Chin, T., 2006. Antimicrobial effects and human gingival biocompatibility of hydroxyapatite sol–gel coatings. J. Biomed. Mater. Res., Part B 76B, 169–178.

Choi, O., Deng, K.K., Kim, N.J., Ross, J.R., Surampalli, R.Y., Hu, Z., 2008. The inhibitory effects of silver nanoparticles, silver ions and silver chloride colloids on microbial growth. Water Res. 42, 3066–3074.

Currey, J., 2001. Biomaterials – sacrificial bonds heal bone. Nature 414, 699–708.

Das, P.K., Pani, S.P., Krishnamoorthy, K., 2000. Prospects of elimination of lymphatic filariasis in India. ICMR Bull 32 (5–6), 41–54.

De With, G., Van Dijk, H.J.A., Hattu, N., Prijs, K., 1981. Preparation, microstructure and mechanical properties of dense polycrystalline hydroxyapatite. J. Mater. Sci. 16, 1592–1598.

Feng, Q.L., Wu, J., Chen, G.Q., Cui, F.Z., Kim, T.N., Kim, T.N., Kim, J.O., 2000. A mechanistic study of the antibacterial effect of silver ions on *E. coli* and *Staphylococcus aureus*. J. Biomed. Mater. Res. 52, 662–668.

Geng, Zhen, Cui, Zhenduo, Li, Zhaoyang, Zhu, Shengli, Liang, Yanqin, William Weijia, Lu, Yang, Xianjin, 2015. Synthesis, characterization and the formation mechanism of magnesium- and strontium-substituted hydroxyapatite. J. Mater. Chem. B 3, 3738.

Gérrard, E., Jai, P., Sridevi, B., Suraj Kumar, T., Mrutyunjay, S., Derek, F., 2016. Kinetic and adsorption behaviour of aqueous cadmium using a 30 nm hydroxyapatite based powder synthesized via a combined ultrasound and microwave based technique. Phys. Chem. 6 (1), 11–22, p-ISSN: 2167-7042.

Gopi, D., Karthika, A., Rajeswari, D., Kavitha, L., Pramod, R., Dwivedi, J., 2014. Investigation on corrosion protection and mechanical performance of minerals substituted hydroxyapatite coating on HELCDEB-treated titanium using pulsed electrodeposition method. RSC Adv. 4, 34751–34759.

Govindarajan, M., 2010. Larvicidal and repellent activities of *Sida acuta Burm*. F. (family: Malvaceae) against three important vector mosquitoes. Asian Pac. J. Trop Med. 3 (9), 691–695.

Guzman, M., Dille, J., Godet, S., 2012. Synthesis and antibacterial activity of silver nanoparticles against gram-positive and gram-negative bacteria. Nanomed. Nanotechnol. Biol. Med. 8, 37–45.

Han, J., Song, H., Saito, F., Lee, B., 2006. Synthesis of high purity nano-sized hydroxy-apatite powder by microwave–hydrothermal method. Mater. Chem. Phys. 99, 235–239.

Iafisco, M., Morales, J.G., Hernandez-Hernandez, M.A., Garcia-Ruiz, J.M., Roveri, N., 2010. Biomimetic carbonate–hydroxyapatite nanocrystals prepared by vapour diffusion. Adv. Eng. Mater. 12 (7), B218–B223.

Iafisco, M., Ruffini, A., Adamiano, A., Sprio, S., Tampieri, A., 2014. Biomimetic magnesium–carbonate-apatite nanocrystals endowed with strontium ions as anti-osteoporotic trigger. Mater. Sci. Eng., C 35, 212–219.

Jiang, H., Jin-Ku, L., Wang, J.D., Lu, Y., Yang, X.H., 2015. Thermal perturbation nucleation and growth of silver molybdate nanoclusters by a dynamic template route. CrystEngComm 17, 5511–5521.

JunfengJia, Huanjun Z., Jie, W., Xin, J., Hong, H., Fangping, C., Shicheng, W., Jung-Woog, S., Changsheng, L., 2010. Development of magnesium calcium phosphate biocement for bone regeneration. J.R. Soc. Interface. http://dx.doi.org/10.1098/rsif.2009.055, 24 February.

Kamaraj, C., Bagavan, A., Rahuman, A.A., Zahir, A.A., Elango, G., Pandiyan, G., 2009. Larvicidal potential of medicinal plant extracts against *Anopheles subpictus Grassi* and *Culex tritaeniorhynchus Giles* (Diptera: Culicidae). Parasitol. Res. 104 (5), 1163–1171.

Kalita, S.J., Verma, S., 2010. Nanocrystalline hydroxyapatite bioceramic using microwave radiation: synthesis and characterization. Mater. Sci. Eng. C 30 (2), 295–303.

Kazin, P.E., Gazizova, O.R., Karpov, A.S., Jansen, M., Tretyakov, Y. D., 2007. Incorporation of 3d-metal ions in the hexagonal channels of the $Sr_5(PO_4)_3OH$ apatite. Solid State Sci. 9, 82–87.

Koumoulidis, G.C., Katsoulidis, A.P., Ladavos, A.K., Pomonis, P.J., Trapalis, C.C., Sdoukos, A.T., Vaimakis, T.C., 2003. Preparation of hydroxyapatite via microemulsion route. J. Colloid Interface Sci., 254–260

Landi, E., Logroscino, G., Proietti, L., Tampieri, A., Sandri, M., Sprio, S., 2008. Biomimetic Mg-substituted hydroxyapatite: from synthesis to in vivo behaviour. J. Mater. Sci., Mater. Med. 19, 239–247.

Lok, C.M., Ho, C.M., Chen, R., He, Q.Y., Yu, W.Y., 2006. Proteomic analysis of the mode of antibacterial action of silver nanoparticles. J. Proteome Res. 5, 916–924.

Landi, E., Tampieri, A., Celotti, G., Sprio, S., 2000. Densification behaviour and mechanisms of synthetic hydroxyapatites. J. Eur. Ceram. Soc. 20 (14–15), 2377–2387.

Liu, J.K., Luo, C.X., Wang, J.D., Yang, X.H., Zhong, X.H., 2012. Controlled synthesis of silver phosphate crystals with high photocatalytic activity and bacteriostatic activity. CrystEngComm 14, 8714–8721.

LeGeros, R.Z., 1991. Calcium phosphates in oral biology and medicine. In: Myers Karger, H. (Ed.), . In: Monographs in Oral Science, vol. 15. AG Publishers, Basel, pp. 82–107.

Mansur, H.S., Costa, H.S., Mansur, A.A.P., Pereira, M., 2012. 3D-macroporous hybrid scaffolds for tissue engineering: network design and mathematical modeling of the degradation kinetics. Mater. Sci. Eng. C 32, 404–415.

Maria, V.R., Daniel, A., 2005. Silicon substituted hydroxyapatite. A method to upgrade calcium phosphate based implants. J. Mater. Chem. 15, 1509–1516.

Pang, Y.X., Bao, X., 2003. Influence of temperature, ripening time and calcination on the morphology and crystallinity of hydroxyapatite nanoparticles. J. Eur. Ceram. Soc. 23, 1697–1704.

Panda, R.N., Hsieh, M.F., Chung, R.J., Chin, T.S., 2003. FTIR, XRD, SEM and solid state NMR investigations of carbonate-containing hydroyapatite nano-particles synthesised by hydroxide-gel technique. J. Phys. Chem. Solids 64 (2), 193–199.

Priyadarshini, K., Murugan, K., Panneerselvam, C., Ponarulselvam, S., Hwang, J.-S., Nicoletti, M., 2012. Biolarvicidal and pupicidal potential of silver nanoparticles synthesized using *Euphorbia hirta* against *Anopheles stephensi* Liston (Diptera: Culicidae). Parasitol. Res. 111 (3), 997–1006.

Rai, M.A., Yadav, A., Gade, A., 2009. Silver nanoparticles as a new generation of antimicrobials. Biotechnol. Adv. 27, 76–83.

Rajakumar, G., Abdul Rahuman, A., 2011. Larvicidal activity of synthesized silver nanoparticles using *Eclipta prostrata* leaf extract against filariasis and malaria vectors. Acta Trop 118 (3), 196–203.

Ragab, H.S., Ibrahim, F.A., Abdallah, F., Al-Ghamdi, A.A., Tantawy, F.E., Yakuphanoglu, F., 2014. Synthesis and in vitro antibacterial properties of hydroxyapatite nanoparticles. J. Pharm. Biol. Sci. 9, 77–85.

Ramanan, S.R., Ramannan, V., 2004. A study of hydroxyapatite fibers prepared via Sol–Gel route. Mater. Lett. 58, 3320–3323.

Rashmi Sanghi, 2000. Microwave irradiation- way to eco-friendly. Green Chem. (March 5), 77–81

Rey, C., 1998. Calcium phosphates for medical applications. In: Amjad, Z. (Ed.), Calcium Phosphates in Biological and Industrial Systems. Kluwer Academic Publisher's, Boston, pp. 217–251.

Russell, S.W., Luptak, K.A., Suchicital, C.T.A., Alford, T.L.A., Pizziconi, V.B., 1996. Chemical and structural evolution of sol–gel-derived hydroxyapatite thin films under rapid thermal processing. J. Am. Ceram. Soc. 79, 837–843.

Sap-Iam, N., Homklinchan, C., Larpudomlert, R., Warisnoicharoen, W., Sereemaspun, A., Dubas, S.T., 2010. UV irradiation induced silver nanoparticles as mosquito larvicides. J. Appl. Sci. 10 (23), 3132–3136.

Sargin, Y., Kizilyalli, M., Telli, C., Guler, H., 1997. A new method for the solidstate synthesis of tetracalcium phosphate: a dental cement: X-ray powder diffraction and IR studies. J. Eur. Ceram. Soc. 17, 963–970.

Santhoshkumar, T., Rahuman, A.A., Rajakumar, G., Marimuthu, S., Bagavan, A., Jayaseelan, C., Zahir, A.A., Elango, G., Kamaraj, C., 2011. Synthesis of silver nanoparticles using *Nelumbo nucifera* leaf extract and its larvicidal activity against malaria and filariasis vectors. Parasitol. Res. 108 (3), 693–702.

Sahayaraj, K., Rajesh, S., 2011. Bionanoparticles: synthesis and antimicrobial applications. In: Mendez-Vilas, A. (Ed.), Science Against Microbial Pathogens; Communicating Current Research and Technological Advances, pp. 228–244.

Sharma, P., Mohan, L., Srivastava, C.N., 2009. *Amaranthus oleracea* and *Euphorbia hirta*: natural potential larvicidal agents against the urban Indian malaria vector, *Anopheles stephensi* Liston (Diptera: Culicidae). Parasitol. Res. 106, 171–176.

Siddharthan, A., Seshadri, A.K., Sampath Kumar, T.S., 2006. Influence of microwave power on nanosized hydroxyapatite particles. Scr. Mater. 55 (2), 175–178.

Sondi, I., Salopek, S.B., 2004. Silver nanoparticles as antimicrobial agent: a case study on *E. coli* as model for Gram negative bacteria. J. Colloid Interface Sci. 275, 177–182.

Stevanovic, M.M., Skapin, S.D., Bracko, I., Milenkovic, M., Petkovic, J., Filipic, M., 2012. Poly (lactide-co-glycolide)/silver nanoparticles: synthesis, characterization, antimicrobial activity, cytotoxicity assessment and ROS-inducing potential. Polymer 53, 2818–2828.

Sun, Y., Guo, G., Wang, Z., Guo, H., 2006. Synthesis of single-crystal HAP nanorods. Ceram. Int. 32 (8), 951–954.

Tas, A.C., 2000. Synthesis of biomimetic Ca–hydroxyapatite powders at 37°C in synthetic body fluids. Biomaterials 21, 1429–1438.

Thamariselvi, T.V., Prabhakaran, K., Rajeshwari, S., 2006. Synthesis of hydroxyapatite that mimic bone minerology trends biomater. Artif. Organs 19 (2), 81–83.

Thompson, J.B., Kindt, J.H., Drake, B., Hansma, H.G., Morse, D.E., Hansma, P.K., 2001. Bone indentation recovery time correlates with bond reforming time. Nature 414, 773–776.

Velmurugan, P., Anbalagan, K., Manosathyadevan, M., Lee, K.J., Cho, M., Lee, S.M., Park, J.H., Oh, S.J., Bang, K.S., Oh, B.T., 2014. Green synthesis of silver and gold nanoparticles using Zingiberofficinale root extract and antibacterial activity of silver nanoparticles against food pathogens. Bioprocess Biosyst. Eng. 37, 1935–1943.

Wang, Y., Zhang, S., Wei, K., Zhao, N., Chen, J., Wang, X., 2006. Hydrothermal synthesis of hydroxyapatite nanopowders using cationic surfactant as a template. Mater. Lett. 60 (12), 1484–1487.

WHO, 1996. Report of the WHO informal consultation on the evaluation on the testing of insecticides. CTD/WHO PES/IC/96.1. WHO, Geneva, p. 69.

WHO—World Health Organization, 2009 Available from: <http://www.who.int/mediacentre/factsheets/fs117/en/index.html>. Accessed April 2012.

World Health Organization, 2010. Dengue Transmission Research in WHO Bulletin. WHO, Geneva.

WHO, 2012. Handbook for Integrated Vector Management. World Health Organization, Geneva.

World Health Organization, 2013. Lymphatic filariasis. <http://www.who.int/mediacentre/factsheets/fs102/en/>.

Zhang, W., Shen, Y., Pan, H., Lin, K., Liu, X., Darvell, B.W., Lu, W. W., Chang, J., Deng, L., Wang, D., Huang, W., 2011. Effects of strontium in modified biomaterials. Acta Biomater. 800.

Zhao, C., Hou, P., Ni, J., Han, P., Chai, Y., Zhang, X., 2016. Ag-incorporated FHA coating on pure mg: degradation and in vitro antibacterial properties. ACS Appl. Mater. Interfaces 8 (8), 5093–5103.

Please cite this article in press as: Udhayakumar, G. et al., Magnesium incorporated hydroxyapatite nanoparticles: Preparation, characterization, antibacterial and larvicidal activity. Arabian Journal of Chemistry (2016), http://dx.doi.org/10.1016/j.arabjc.2016.05.010